

## A Dual-Mode HDAC Prodrug for Covalent Modification and Subsequent Inhibitor Release

Kevin B Daniel, Eric D Sullivan, Yao Chen, Joshua C. Chan,  
Patricia A. Jennings, Carol A. Fierke, and Seth M. Cohen

*J. Med. Chem.*, **Just Accepted Manuscript** • DOI: 10.1021/acs.jmedchem.5b00539 • Publication Date (Web): 14 May 2015

Downloaded from <http://pubs.acs.org> on May 18, 2015

### Just Accepted

“Just Accepted” manuscripts have been peer-reviewed and accepted for publication. They are posted online prior to technical editing, formatting for publication and author proofing. The American Chemical Society provides “Just Accepted” as a free service to the research community to expedite the dissemination of scientific material as soon as possible after acceptance. “Just Accepted” manuscripts appear in full in PDF format accompanied by an HTML abstract. “Just Accepted” manuscripts have been fully peer reviewed, but should not be considered the official version of record. They are accessible to all readers and citable by the Digital Object Identifier (DOI®). “Just Accepted” is an optional service offered to authors. Therefore, the “Just Accepted” Web site may not include all articles that will be published in the journal. After a manuscript is technically edited and formatted, it will be removed from the “Just Accepted” Web site and published as an ASAP article. Note that technical editing may introduce minor changes to the manuscript text and/or graphics which could affect content, and all legal disclaimers and ethical guidelines that apply to the journal pertain. ACS cannot be held responsible for errors or consequences arising from the use of information contained in these “Just Accepted” manuscripts.

1  
2  
3  
4  
5  
6  
7  
8  
9  
10  
11  
12  
13  
14  
15  
16  
17  
18  
19  
20  
21  
22  
23  
24  
25  
26  
27  
28  
29  
30  
31  
32  
33  
34  
35  
36  
37  
38  
39  
40  
41  
42  
43  
44  
45  
46  
47  
48  
49  
50  
51  
52  
53  
54  
55  
56  
57  
58  
59  
60

# A Dual-Mode HDAC Prodrug for Covalent Modification and Subsequent Inhibitor Release

*Kevin B. Daniel,<sup>1</sup> Eric D. Sullivan,<sup>2</sup> Yao Chen,<sup>1</sup> Joshua C. Chan,<sup>1</sup> Patricia A. Jennings,<sup>1</sup> Carol A. Fierke,<sup>2,3,4\*</sup> and Seth M. Cohen<sup>1\*</sup>*

<sup>1</sup>Department of Chemistry and Biochemistry, University of California, San Diego, La Jolla, CA  
92093, United States

<sup>2</sup>Interdepartmental Program in Chemical Biology, <sup>3</sup>Department of Biological Chemistry, and

<sup>4</sup>Department of Chemistry, University of Michigan, Ann Arbor, MI 48109, United States

1  
2  
3 ABSTRACT. Histone deacetylase inhibitors (HDACi) target abnormal epigenetic states  
4 associated with a variety of pathologies including cancer. Here, the development of a prodrug of  
5 the canonical broad-spectrum HDACi suberoylanilide hydroxamic acid (SAHA) is described.  
6  
7  
8 Although hydroxamic acids are utilized universally in the development of metalloenzyme  
9 inhibitors, they are considered poor pharmacophores with reduced activity in vivo. We  
10 developed a prodrug of SAHA by appending a promoiety, sensitive to thiols, to the hydroxamic  
11 acid warhead (termed SAHA-TAP). After incubation of SAHA-TAP with an HDAC, the thiol of  
12 a conserved HDAC cysteine residue becomes covalently tagged with the promoiety, initiating a  
13 cascade reaction that leads to the release of SAHA. Mass spectrometry and enzyme kinetics  
14 experiments validate that the cysteine residue is covalently appended with the TAP promoiety.  
15  
16  
17 SAHA-TAP demonstrates cytotoxicity activity against various cancer cell lines. This strategy  
18 represents an original prodrug design with a dual-mode of action for HDAC inhibition.  
19  
20  
21  
22  
23  
24  
25  
26  
27  
28  
29  
30  
31  
32  
33  
34  
35  
36  
37  
38  
39  
40  
41  
42  
43  
44  
45  
46  
47  
48  
49  
50  
51  
52  
53  
54  
55  
56  
57  
58  
59  
60

1  
2  
3 Transcription is a tightly regulated biological process that is the first step in gene expression.<sup>1-3</sup>  
4  
5 In eukaryotic cells, sequence-specific DNA binding factors control the flow of genetic  
6  
7 information from DNA to RNA, thereby regulating transcription. In cells, DNA is tightly  
8  
9 compacted into chromatin, a highly organized and dynamic complex between DNA and proteins.  
10  
11 When gene transcription is activated, the DNA is made accessible to transcription factors via  
12  
13 nucleosome modification.<sup>1, 2</sup> The local architecture of chromatin, which is influenced by post-  
14  
15 translational modifications of histones, can regulate gene expression. These modifications  
16  
17 include methylation, phosphorylation, and acetylation of core histones. Histone acetylation  
18  
19 occurs at the  $\epsilon$ -amino groups of conserved lysine residues near the N-termini. Acetylation levels  
20  
21 of core histones are a result of the balance between histone acetyltransferases (HATs) and  
22  
23 histone deacetylases (HDACs).<sup>1-4</sup> Increased levels of histone acetylation are generally associated  
24  
25 with transcriptional activity, whereas decreased levels of histone acetylation are associated with  
26  
27 repression of transcription. Additionally, acetylation of specific lysines on histone tails  
28  
29 facilitates the recruitment of bromodomain-containing chromatin remodeling factors.<sup>5, 6</sup>  
30  
31 Furthermore, acetylated lysines have been observed in many cellular proteins indicating that  
32  
33 HATs and HDACs do not function solely to modify histones.<sup>7</sup>  
34  
35  
36  
37  
38  
39  
40

41 Histone deacetylase inhibitors (HDACi) have been developed as a class of therapeutic agents  
42  
43 intended to target aberrant epigenetic states associated with a variety of pathologies, most  
44  
45 notably cancer.<sup>8</sup> Recent findings have shown that the relief of oncogenic transcriptional  
46  
47 repressors by HDACi can lead to cell cycle arrest and apoptosis.<sup>1-4</sup> This is because many cancers  
48  
49 have evolved such that pro-apoptotic pathways are transcriptionally repressed via histone  
50  
51 deacetylation. HDACi prevent deacetylation of the lysine residues of the histone tails, which in  
52  
53 turn leads to transcriptional activation, gene expression, and cell death.<sup>1, 8</sup>  
54  
55  
56  
57  
58  
59  
60

1  
2  
3 The development of HDACi has been ongoing, and >10 candidates have progressed to clinical  
4 trials.<sup>3</sup> HDACi can be subdivided into structural classes including hydroxamic acids, cyclic  
5 peptides, aliphatic acids, and benzamides.<sup>9</sup> The HDACi Vorinostat (suberoylanilide hydroxamic  
6 acid, SAHA) received approval by the United States Food and Drug Administration (FDA) in  
7 2006 for the treatment of cutaneous T-cell lymphoma (CTCL).<sup>10</sup> Crystallization of SAHA with  
8 HDAC8 supported a model involving the linkage of a metal-binding pharmacophore (MBP) to a  
9 capping group designed to form favorable interactions with amino acid residues at the entrance  
10 to the active site tunnel (Figure 1a).<sup>11</sup> Three other HDACi have been approved by the FDA  
11 including Panobinostat and Belinostat, both broad-spectrum, hydroxamate-based HDACi for the  
12 treatment of multiple myeloma or relapsed/refractory peripheral T-cell lymphoma, respectively  
13 (Figure 1a).<sup>12, 13</sup> Romidepsin (FK228), a cyclic peptide HDACi that uses a thiol group to  
14 coordinate the active site metal ion, is approved for CTCL treatment (Figure 1a).<sup>10</sup>

15  
16  
17  
18  
19  
20  
21  
22  
23  
24  
25  
26  
27  
28  
29  
30  
31  
32  
33  
34  
35  
36  
37  
38  
39  
40  
41  
42  
43  
44  
45  
46  
47  
48  
49  
50  
51  
52  
53  
54  
55  
56  
57  
58  
59  
60  
SAHA, Romidepsin, and Panobinostat act to inhibit most isoforms of the metal-dependent  
HDAC family and are regarded as broad-spectrum HDAC inhibitors. Despite promising clinical  
results for HDACi, these drugs have not been effective in clinical trials involving solid tumors.  
In fact, these FDA-approved drugs have been associated with the onset of serious side effects  
including: fatigue, gastrointestinal issues (diarrhea, nausea, vomiting), and hematologic  
complications (thrombocytopenia, anemia, neutropenia).<sup>8, 10</sup> Both SAHA and Romidepsin have  
also been associated with cardiotoxicity.<sup>8</sup> Clinical studies in humans determined the major  
metabolic pathways of SAHA degradation involve glucuronidation by UDP-  
glucuronosyltransferases (UGTs) to generate inactive **1** (Figure 1b). Alternatively, hydrolysis of  
SAHA to the carboxylic acid analog (**2**), followed by  $\beta$ -oxidation generates the inactive  
metabolite 4-anilino-4-oxobutanoic acid (**3**, Figure 1b).<sup>10, 14</sup> Clinical studies determined that the

mean steady state serum exposures of **1** and **2** were 4-fold and 13-fold higher than SAHA, respectively. Additionally, the apparent  $t_{1/2}$  of SAHA in human serum was  $\sim 1.5$  h for patients receiving single doses of 400 mg SAHA.<sup>8, 10, 14</sup> The poor pharmacokinetic (PK) properties of SAHA are similar for other hydroxamic acid-based compounds and involve chemical instability and rapid elimination.<sup>8, 15</sup> In fact, the FDA has approved SAHA for CTCL only in patients with persistent or recurrent disease who have already followed two systemic therapies.<sup>8</sup> Similarly, the FDA has only approved Romidepsin for CTCL treatment in patients who have received at least one prior systemic therapy, and Panobinostat is only administered after two prior standard therapies have failed.<sup>16</sup> The onset of these deleterious side effects is proposed to originate, in part, from the lack of selectivity of these drugs for a specific HDAC isozyme.<sup>8</sup>

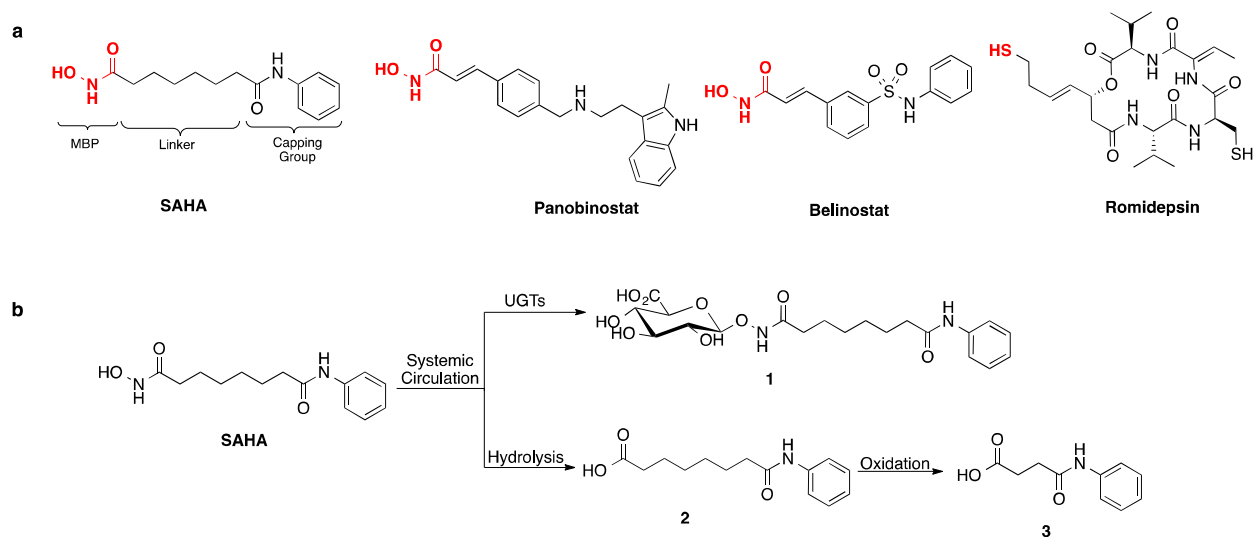


**Figure 1.** FDA-approved HDAC inhibitors. (a) The hydroxamic acid and sulfhydryl MBP donor atoms of SAHA, Panobinostat, Belinostat, and Romidepsin are shown in red. (b) Metabolism of SAHA. Upon systemic circulation, UGT enzymes localized in the liver can convert SAHA to a SAHA  $\beta$ -D-glucuronide (**1**) rendering the drug inactive. A different pathway

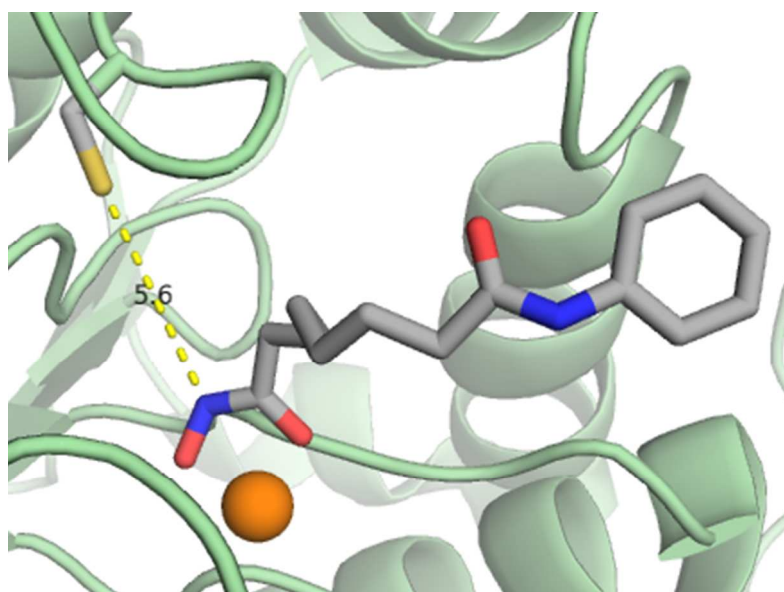
1  
2  
3 involves initial hydrolysis of SAHA to the corresponding carboxylic acid (**2**), followed by  
4  
5 oxidation to **3**.  
6  
7  
8  
9

10  
11 Chemically modified versions of active drugs have been developed in an effort to overcome  
12 barriers to drug formulation and delivery. The modified, latent version of the drug, termed the  
13 prodrug, undergoes a transformation in the presence of a desired chemical or enzymatic stimulus  
14 in vivo to generate the active agent.<sup>17, 18</sup> The chemical group appended to the active drug  
15 rendering it inactive is termed the promoiety. Only a handful of reports have investigated HDAC  
16 prodrugs, with most studies focused on developing acyl derivatives of SAHA or similar  
17 hydroxamic acid-based HDACi to enhance cell permeability and hydrolytic stability.<sup>19</sup> As  
18 expected, these prodrugs showed little activity as HDAC inhibitors and biochemical assays  
19 suggest that the acylated prodrugs are more cell-permeable than the hydroxamic acid parent  
20 drugs. A similar report investigated a carbamate prodrug concept for hydroxamate HDACi  
21 (including SAHA) to improve drug-like properties, including cellular permeability.<sup>20</sup> However,  
22 both of these strategies rely on hydrolysis in vivo to release the active drug and do not improve  
23 drug-target specificity for selected disease states or sites of disease.  
24  
25  
26  
27  
28  
29  
30  
31  
32  
33  
34  
35  
36  
37  
38  
39  
40  
41

42 Initially, we sought to develop new HDAC inhibitor prodrugs (proinhibitors) that become  
43 activated in the presence of thiols such as glutathione in its reduced form (GSH), which is  
44 frequently more abundant at the site of disease (e.g. cancer).<sup>21</sup> Previously, Huang and coworkers  
45 reported the development of a long-wavelength fluorescent probe involving a quinone-methide  
46 reaction that can detect physiologically relevant thiols including GSH.<sup>22</sup> Although the quinone  
47 promoiety functions as an electrophilic Michael acceptor, it was determined that other  
48 biologically relevant nucleophiles, including serine and lysine, were unreactive with this  
49  
50  
51  
52  
53  
54  
55  
56  
57  
58  
59  
60

1  
2  
3 functionality. Our prodrug approach considered the covalent appendage of this quinone  
4  
5  
6 promoiety to the hydroxamate of an HDACi, since the alkylation of hydroxamates has shown to  
7  
8  
9 be effective in improving PK properties including hydrolytic stability, cellular permeability, and  
10  
11 glucoronidation.<sup>19, 23, 24</sup>

12  
13 As described below, we found that even in the absence of nucleophilic thiols, we observed  
14  
15 activation of our prodrug (SAHA-TAP); sequence homology analysis revealed a single cysteine  
16  
17 (Cys) residue is conserved in all metal-dependent HDAC isoforms, which we found was reactive  
18  
19 with our prodrug (Supporting Information, Figure S1).<sup>25</sup> The crystal structure of HDAC8  
20  
21 complexed with SAHA reveals that the conserved Cys (Cys153 for HDAC8) is located in the  
22  
23 catalytic active site pocket ~5.6 Å away from the hydroxamic acid moiety of SAHA (Figure 2).  
24  
25 Thus, we have concluded that our prodrug is cleaved by the sulfhydryl moiety of the conserved  
26  
27 Cys of HDAC, leading to drug activation and a dual mode of inhibition: covalent modification of  
28  
29 the conserved Cys leading to the formation of an inactive, covalently modified enzyme and  
30  
31 release of the competitive inhibitor SAHA.  
32  
33  
34  
35  
36  
37  
38  
39  
40  
41  
42  
43  
44  
45  
46  
47  
48  
49  
50  
51  
52  
53  
54  
55  
56  
57  
58  
59  
60





1  
2  
3 **Figure 2.** Protein crystal structure of HDAC8 complexed with SAHA. The distance between  
4 the sulfhydryl moiety of Cys153 and the nitrogen atom of the MBP of SAHA was determined to  
5 be 5.6 Å. SAHA and Cys153 are shown as sticks in color code (carbon = grey, nitrogen = blue,  
6 oxygen = red, sulfur = yellow) and the Zn<sup>2+</sup> ion is shown as an orange sphere (PDB: 1T69).  
7  
8  
9  
10  
11  
12  
13  
14  
15

## 16 **Results and Discussion**

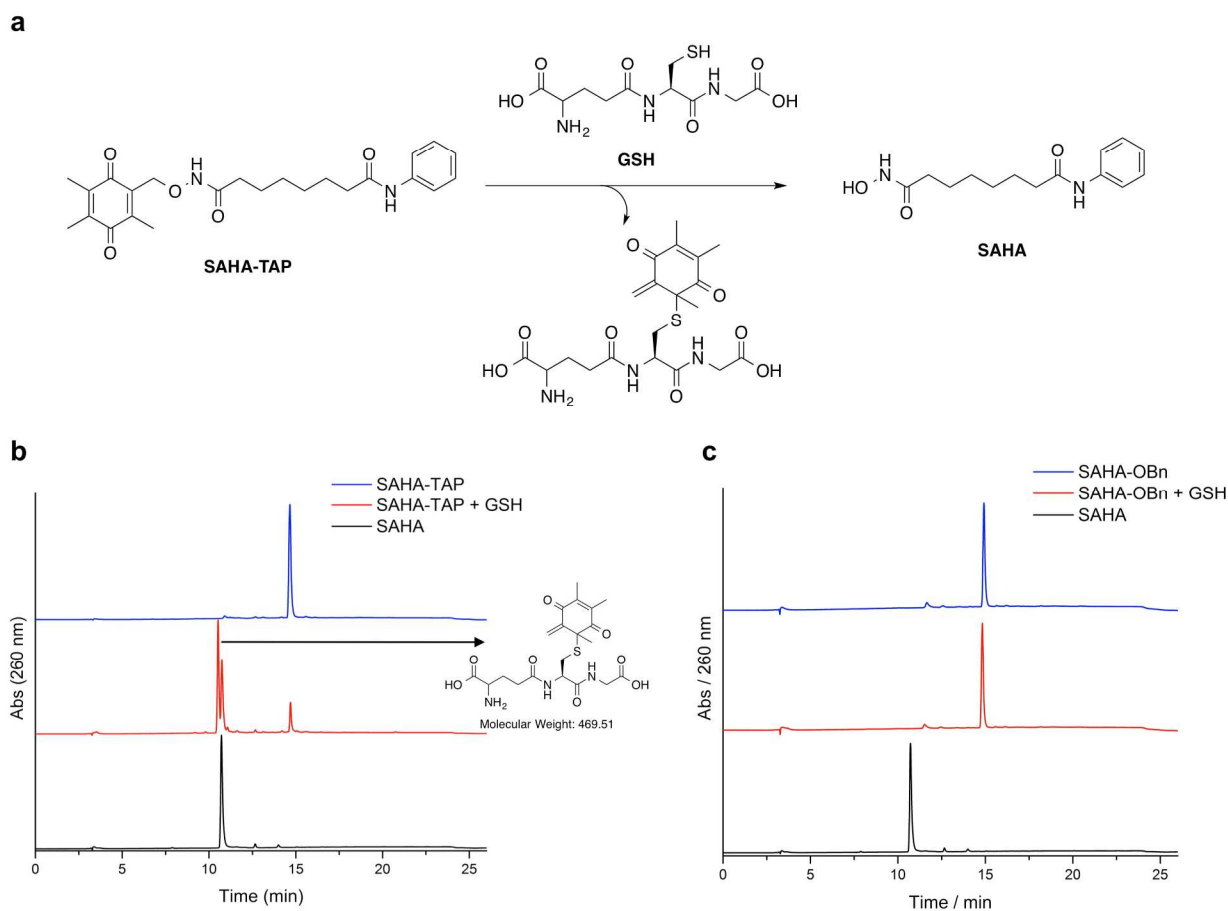
### 17 **Development of a Unique HDACi Prodrug.**

18  
19  
20 SAHA was chosen as the drug of interest because it is FDA-approved for the treatment of  
21 CTCL and has been well studied. A prodrug of SAHA containing a quinone-based, thiol-  
22 sensitive promoiety was designed, termed SAHA-TAP (TAP = thiol activated prodrug) (Figure  
23 3). To develop SAHA-TAP, the promoiety was first synthesized using a modified literature  
24 procedure.<sup>22</sup> The promoiety was appended to SAHA under basic conditions to generate SAHA-  
25 TAP. A control compound, SAHA-OBn, was synthesized in a similar manner. This compound  
26 contains a benzyl moiety appended to SAHA via the *N*-hydroxyl functionality. SAHA-OBn was  
27 designed to have a similar structure to SAHA-TAP, but to be unreactive toward nucleophilic  
28 thiols.  
29  
30  
31  
32  
33  
34  
35  
36  
37  
38  
39  
40  
41  
42  
43

### 44 **Assessment of SAHA-TAP Reactivity with GSH.**

45  
46 To evaluate the reactivity of SAHA-TAP and SAHA-OBn with nucleophilic thiols, analytical  
47 HPLC was utilized under simulated physiological conditions (50 mM HEPES, pH 7.4). SAHA-  
48 TAP was treated with GSH (2 mM, 2 eq) to confirm that the prodrug is indeed reactive with  
49 thiols. After incubation of SAHA-TAP with GSH, three distinct peaks were apparent in the  
50 HPLC chromatogram (Figure 3a). Liquid chromatography-mass spectrometry (LCMS) confirms  
51  
52  
53  
54  
55  
56  
57  
58  
59  
60

1  
2  
3 that the identity of the first peak ( $R_t = 10.5$  min) is the quinone-methide side product, the second  
4 peak is SAHA ( $R_t = 10.7$  min) and the third peak is unreacted SAHA-TAP ( $R_t = 14.7$  min).  
5  
6  
7  
8 Treatment of SAHA-OBn with GSH under the same conditions resulted in no change in the  
9  
10 HPLC chromatogram, indicative of the expected lack of reactivity (Figure 3b). Having shown  
11  
12 that SAHA-TAP reacts rapidly with GSH, the aqueous stability of SAHA-TAP was evaluated  
13  
14 under simulated physiological conditions (50 mM HEPES, pH 7.4). An HPLC chromatogram  
15  
16 was obtained immediately after preparation in aqueous buffer and a second trace was collected  
17  
18 after incubation at 37 °C for 24 h. SAHA-TAP was determined to be >97% stable to hydrolysis  
19  
20 in the absence of thiols (Figure S2). The activation of SAHA-TAP by reaction with GSH is  
21  
22 summarized in Figure 3c.  
23  
24  
25  
26  
27



1  
2  
3 **Figure 3.** (a) Activation of SAHA-TAP by GSH. In the presence of GSH, the sulfhydryl moiety  
4 can attack the electrophilic quinone moiety. Subsequent rearrangement releases SAHA along  
5 with a quinone-methide adduct. (b) HPLC trace of SAHA (black), SAHA-TAP (blue), and  
6 SAHA-TAP after treatment with GSH (2 mM, 2 eq) for 2 h at 37 °C (red). Retention times are  
7 10.7 min for SAHA, 14.7 min for SAHA-TAP, and 10.5 min for the quinone-methide GSH  
8 adduct generated from the reaction. (c) HPLC trace of SAHA (black), SAHA-OBn (blue), and  
9 SAHA-OBn after incubation in HEPES (50 mM, pH 7.4) for 24 h at 37 °C (red). Retention  
10 times are 10.7 min for SAHA and 14.9 min for SAHA-OBn.  
11  
12  
13  
14  
15  
16  
17  
18  
19  
20  
21  
22  
23  
24  
25

### 26 **HDAC Inhibition by SAHA-TAP.**

27  
28 To determine the efficacy of the SAHA-TAP prodrug strategy, the ability of SAHA-TAP and  
29 SAHA-OBn to inhibit HDAC-1, -2, -3, -6, and -8 was evaluated using an optimized homogenous  
30 fluorescence-based assay (BPS Bioscience). Surprisingly, even in the absence of exogenous  
31 thiols, SAHA-TAP was an effective inhibitor of all HDACs tested with an apparent  $IC_{50}$  value  
32 that is slightly less potent (2- to 50-fold) than the parent inhibitor SAHA (Table S1). This result  
33 was unexpected because the metal-binding ability of the hydroxamic acid MBP of SAHA-TAP is  
34 blocked by the promoiety, which should render the drug nearly inactive. Recent studies indicate  
35 that the metal-free form of HDAC8 has a low affinity for SAHA analogs, further demonstrating  
36 the importance of metal binding for HDAC inhibition.<sup>26</sup> To determine if a component of the  
37 biochemical assay resulted in SAHA-TAP activation, analytical HPLC was utilized. SAHA-  
38 TAP was incubated with either BSA (5 mg/mL) or trypsin (5 mg/mL) at 37 °C for 2 h; however,  
39 SAHA-TAP was found to be >95% stable in the presence of either of these assay components  
40 (data not shown).  
41  
42  
43  
44  
45  
46  
47  
48  
49  
50  
51  
52  
53  
54  
55  
56  
57  
58  
59  
60

1  
2  
3 Because SAHA-TAP is a larger molecule than SAHA and the metal-binding hydroxamate  
4 group is blocked, it is feasible that the promoiety may be positioned very close to Cys153 when  
5 bound to HDAC8. This positioning could be ideal for nucleophilic attack by the sulfhydryl  
6 moiety, leading to covalent modification and SAHA release. We hypothesized that the Cys153  
7 residue of HDAC8 reacts with bound SAHA-TAP, resulting in a covalent modification of the  
8 protein and subsequent release of SAHA, a competitive inhibitor (Figure S3). It is important to  
9 note that there are many other Cys residues in the metal-dependent HDAC isoforms (e.g. 10 Cys  
10 residues in HDAC8), and activation of SAHA-TAP by these residues may also be responsible in  
11 part for the release of SAHA we observe (vide supra).  
12  
13  
14  
15  
16  
17  
18  
19  
20  
21  
22  
23  
24  
25  
26

### 27 **Mass Spectrometry Analysis**

28  
29 To investigate whether the active site Cys153 is covalently modified by the SAHA-TAP  
30 promoiety, mass spectrometry (MS) techniques were utilized. Digestion of wild type (WT)  
31 HDAC8 with trypsin yields an 18 amino acid peptide containing Cys153, which can be used to  
32 monitor the modification via mass spectrometry (Figure 4a). If a covalent modification occurs at  
33 this position after treatment of WT HDAC8 with SAHA-TAP, the expected MS ion for this  
34 peptide fragment will be different from the unmodified parent ion.  
35  
36  
37  
38  
39  
40  
41  
42

43 HDAC8 (WT, with or without incubation with a 12-fold excess of SAHA-TAP for 60 min at  
44 37 °C) was digested with trypsin, and the resulting peptides were analyzed by LCMS. The  
45 expected parent ion for the WT HDAC8 Cys153 peptide was consistent with a peak at  $R_t = 84.5$   
46 min (Figure 4b). Similarly, a peak at  $R_t = 88.5$  min corresponds to the expected parent ion for  
47 the covalently modified Cys153 HDAC8 peptide after SAHA-TAP treatment (Figure 4c). To  
48  
49  
50  
51  
52  
53  
54  
55  
56  
57  
58  
59  
60

eliminate other digestion products that could account for this ion, further MS techniques were applied to verify that these ion peaks correspond to the peptide sequence of interest.

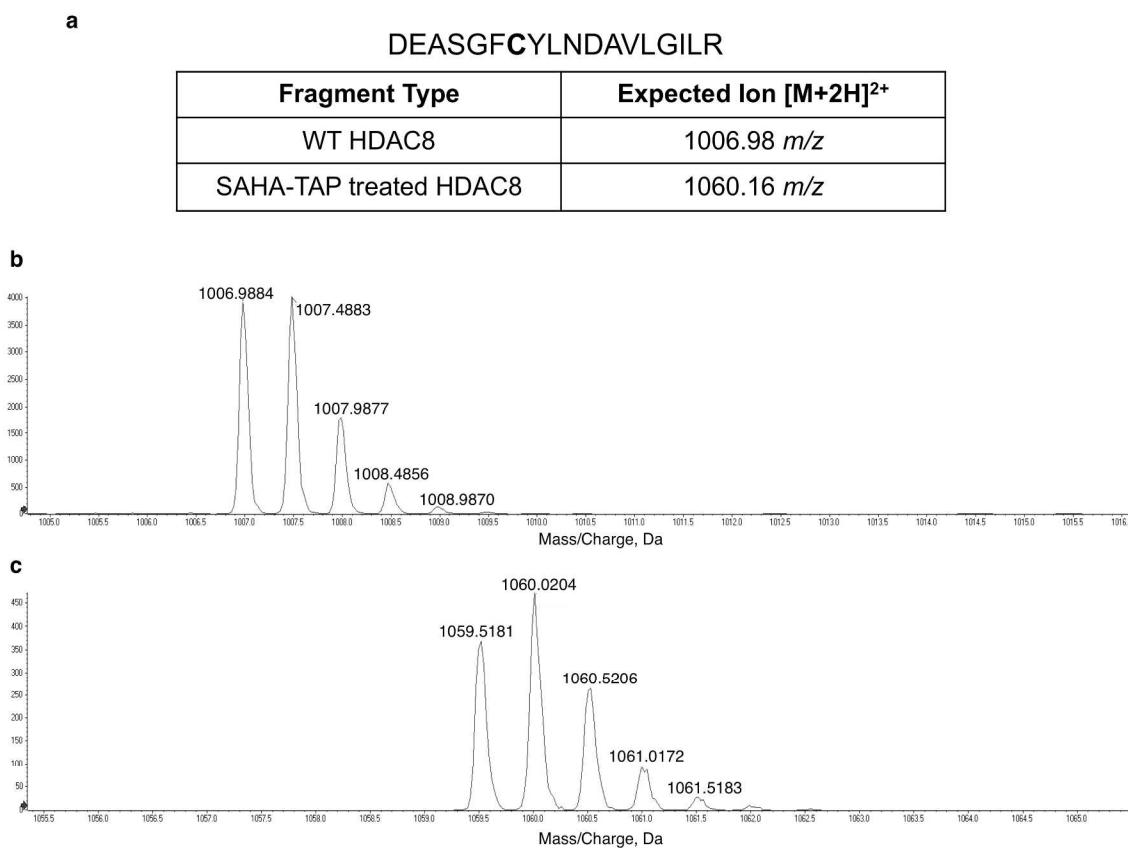


**Figure 4.** HDAC8 tryptic fragment MS data. (a) Expected HDAC8 Cys153 peptide upon digestion with trypsin (Cys153 in bold). The expected MS ion for the WT protein is shown along with the expected ion for the peptide including the covalent addition of the TAP promoiety on Cys153. (b) The tryptic fragment of WT HDAC8 ( $R_t = 84.5$  min) is consistent with the expected  $[M+2H]^{2+}$  ion. (c) After treatment of HDAC8 with SAHA-TAP (12 eq) and digestion with trypsin, a peak aligning with the expected  $[M+2H]^{2+}$  ion is observed ( $R_t = 88.5$  min).

1  
2  
3 Tandem mass spectrometry (MS<sup>2</sup> or MS/MS) is routinely used in proteomics to characterize  
4 amino acid sequences of proteins, where peptides undergo further fragmentation to amino acid  
5 aggregates.<sup>27</sup> The fragmentation patterns observed in the MS/MS spectra of tryptic peptides for  
6 WT HDAC8 and SAHA-TAP treated HDAC8 were investigated to obtain additional insight into  
7 the possibility of covalent modification of Cys153. The expected monoisotopic masses for the *y*  
8 ion series in both WT HDAC8 and the SAHA-TAP treated sample are summarized in Table S2.  
9  
10 The expected *y* fragment ions for both peptides align until Cys153 (*y*<sub>12</sub>), where this ion and each  
11 subsequent ion have different masses. Indeed, the MS/MS fragmentation spectrum for the WT  
12 HDAC8 tryptic peptide (parent ion *m/z*=1006.98, [M+2H]<sup>2+</sup>) shows many of the expected *y* ions  
13 (Figure S4). Similarly, the MS/MS fragmentation spectrum for the SAHA-TAP treated HDAC8  
14 tryptic peptide (parent ion *m/z*=1059.53 [M+2H]<sup>2+</sup>) shows many *y* ions including the  
15 characteristic peak of *m/z*=1511.82 (Figure S5). This peak is indicative of a covalent  
16 modification of *m/z*=162.1 for the HDAC8 tryptic fragment at Cys153. These data prove that the  
17 covalent modification of Cys153 is occurring to form an adduct containing the SAHA-TAP  
18 promoiety, as shown in Fig. 2c.

19  
20 MS analysis also indicated that Cys102, Cys244, and Cys314 could be modified by the TAP  
21 moiety from SAHA-TAP. Importantly, the peptides containing surface cysteines (Cys275 and  
22 Cys352) were not modified with TAP, suggesting that activation is not non-specific.  
23  
24 Nonetheless, the hypothesized mechanism of activation involving a covalent modification of Cys  
25 residues in HDAC8, including Cys153, was observed, which can aid in explaining the inhibition  
26 of HDACs by SAHA-TAP even in the absence of exogenous nucleophilic thiols, as observed in  
27 the *in vitro* assays.

### In vitro Time Dependence of SAHA-TAP HDAC Inhibition.

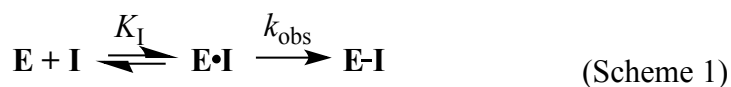
With the MS data in hand confirming covalent modification of Cys residues in HDAC8, we sought to investigate the kinetics of inhibition of HDAC8 by SAHA-TAP using the Fluor-de-Lys activity assay (Enzo Life Sciences). A previous study determined that the catalytic activity and thus inhibition of HDAC8 is dependent on the identity of the active site metal ion (e.g.  $\text{Co}^{2+}$ ,  $\text{Fe}^{2+}$ ,  $\text{Zn}^{2+}$ , and  $\text{Ni}^{2+}$ ).<sup>28</sup> To obtain the most accurate results, apo-HDAC8 (human, recombinant) was initially prepared before the addition of  $\text{Zn}^{2+}$  in a 1:1 stoichiometry. An initial test of HDAC8 inhibition by preincubation of the enzyme with SAHA-TAP demonstrated that activity loss occurred within the first 0.5 h (data not shown). To determine the kinetics for the time-dependent inhibition by SAHA-TAP, HDAC8 progress curves were measured through a range of inhibitor concentrations (Figure 5a). For these reactions, the Fluor-de-Lys HDAC8 substrate (150  $\mu\text{M}$ ) and SAHA-TAP (0-20  $\mu\text{M}$ ) were added to each assay prior to initiating the reactions with WT HDAC8 (0.5  $\mu\text{M}$ ). Over a time course, aliquots of the reactions were stopped by dilution into a solution of Trichostatin A and trypsin, and product formation was analyzed from the resulting change in fluorescence. Analysis of the HDAC8 progress curves in the presence of increasing concentrations of SAHA-TAP demonstrates a non-linear formation of product with respect to time. Equation 1, which describes the time-dependent decrease in initial velocity under steady state turnover conditions,<sup>29, 30</sup> was fit to the progress curves:

$$P = \frac{(v_s * t) + (v_0 - v_s) * [1 - \exp(-k_{obs} * t)]}{k_{obs} + C} \quad (\text{Equation 1})$$

where  $P$  represents production formation,  $v_s$  and  $v_0$  represent final and initial velocities, respectively,  $t$  is time,  $C$  is the initial fluorescent ratio, and  $k_{obs}$  is the rate constant describing the

1  
2  
3 transition from the initial velocity to the final steady state velocity, reflecting the time-dependent  
4  
5 enzyme inactivation.  
6

7  
8 This fit reveals that both the initial velocity and the rate constant for inactivation,  $k_{\text{obs}}$ , have a  
9  
10 hyperbolic dependence on the concentration of SAHA-TAP (Figures 5b-c). The initial velocity  
11  
12 decreases with an apparent  $K_i = 7 \pm 4 \mu\text{M}$  and the rate constant for inactivation increases with a  
13  
14  $K_{1/2} = 8 \pm 2 \mu\text{M}$  to a maximal rate constant of  $0.0013 \text{ s}^{-1}$  at saturating SAHA-TAP. This type of  
15  
16 inhibition is characteristic of a two-step mechanism (Scheme 1) in which a rapid reversible step,  
17  
18 such as binding of SAHA-TAP to HDAC8, is followed by a time dependent step, consistent with  
19  
20 irreversible inactivation.<sup>29, 30</sup> These data demonstrate that the prodrug, SAHA-TAP, is capable  
21  
22 of binding to and inhibiting HDAC8. The time-dependent decrease in activity is consistent with  
23  
24 the MS data demonstrating the formation of a covalent enzyme adduct.  
25  
26  
27  
28  
29  
30  
31



32  
33  
34  
35  
36  
37  
38 For comparison, progress curves for inhibition of HDAC8 with the competitive inhibitor  
39  
40 SAHA and a negative control, SAHA-OBn, were evaluated. These assays were performed in the  
41  
42 same manner as the SAHA-TAP progress curves, where substrate and inhibitor were added to  
43  
44 the assay prior to the addition of HDAC8 to initiate the reaction. In contrast to the data with  
45  
46 SAHA-TAP, these progress curves are linear with no observable curvature for all concentrations  
47  
48 of SAHA (Figure S6a) and SAHA-OBn (Figure S6b). As expected, HDAC8 ( $0.5 \mu\text{M}$ ) is  
49  
50 inhibited >90% by SAHA in the concentration range tested ( $2\text{-}8 \mu\text{M}$ ), which is in agreement with  
51  
52 the  $250 \text{ nM } K_i$  reported for  $\text{Zn}^{2+}$ -HDAC8.<sup>28</sup> SAHA-OBn ( $2\text{-}10 \mu\text{M}$ ) does not inhibit the activity  
53  
54 of HDAC8. The lack of inhibition by SAHA-OBn is consistent with previous  $\text{IC}_{50}$  data (Table  
55  
56  
57  
58  
59  
60



1  
2  
3 S1). Taken together, these data show that SAHA-TAP has a unique mode of inhibition for  
4 HDAC8 when compared to SAHA. This inhibitor functions both as a competitive inhibitor, and  
5  
6 as a time-dependent inactivator, in contrast to the linear, time-independent inhibition observed  
7  
8 for SAHA.  
9  
10

11  
12 To determine the role of Cys153 on the time dependent inhibition of HDAC8, a Cys153Ala  
13 (C153A) HDAC8 mutant was prepared and purified. In vitro assays for the mutant were  
14  
15 conducted under the same conditions used for WT HDAC8. Progress curves for these assays  
16  
17 reveal dose-responsive inhibition with  $K_i = 8 \pm 4 \mu\text{M}$  for SAHA-TAP (Figure 5d and Figure S7).  
18  
19 Furthermore, these progress curves are linear for all concentrations of inhibitor, showing a loss  
20  
21 of the time-dependent inhibition observed with WT HDAC8. This data suggests that SAHA-  
22  
23 TAP, containing the same linker spacer and capping group as SAHA, can bind HDAC8 in a non-  
24  
25 covalent manner, inhibiting the enzyme (Scheme 1). The linear progress curves also  
26  
27 demonstrate that Cys153 is important for the time-dependent inactivation, eliminating an  
28  
29 alternate explanation that the time-dependent inhibition is due to the slow formation of SAHA  
30  
31 from SAHA-TAP. Progress curves with C153A HDAC8 measured with SAHA and SAHA-OBn  
32  
33 data reveal that the HDAC8 mutant remains susceptible to inhibition by SAHA and not SAHA-  
34  
35 OBn (Figure S8).  
36  
37  
38  
39  
40  
41  
42

43  
44 Collectively, these data indicate both that SAHA-TAP binds non-covalently to HDAC8 to  
45  
46 inhibit the activity and that the time-dependence mainly reflects the reaction of SAHA-TAP with  
47  
48 Cys153. Although the MS data suggests that SAHA-TAP can react with other Cys residues in  
49  
50 HDAC8 leading to SAHA release, C153A HDAC8 is not inactivated in a time-dependent  
51  
52 manner, demonstrating the importance of this particular Cys in the mechanism of inhibition for  
53  
54 the WT enzyme. The combination of the enzyme kinetics and MS data provides evidence that  
55  
56  
57  
58  
59  
60

the inactivation of HDAC8 by SAHA-TAP involves two steps: non-covalent binding of SAHA-TAP to HDAC8 followed by covalent modification of Cys153.

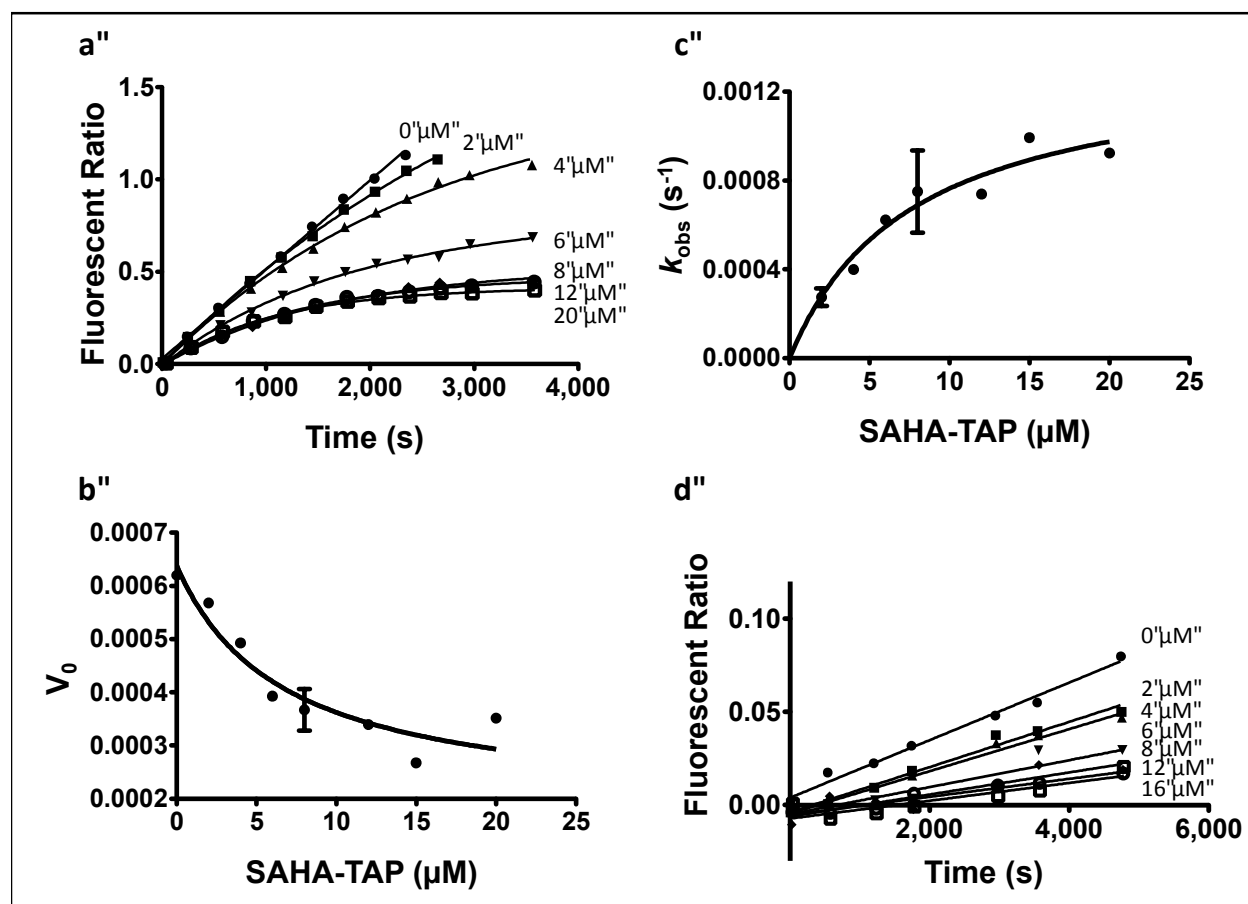


**Figure 5.** Time dependence of HDAC8 inhibition. (a) WT HDAC8 (0.5  $\mu\text{M}$ ) progress curves at varying concentrations (0-20  $\mu\text{M}$ ) of SAHA-TAP. Dependence of both the (b) initial rate,  $v_0$ , and (c)  $k_{obs}$  on the concentration of SAHA-TAP. (d) C153A HDAC8 (2  $\mu\text{M}$ ) progress curves at varying concentrations (0-20  $\mu\text{M}$ ) of SAHA-TAP.

### Plasma Stability

As mentioned earlier, SAHA suffers from poor PK properties, including hydrolytic instability with  $t_{1/2} \sim 1.5$  h. To determine the stability of SAHA-TAP in a biologically relevant model,

1  
2  
3 human plasma stability studies were conducted as previously reported.<sup>31</sup> After incubating SAHA  
4 or SAHA-TAP in human plasma, aliquots were withdrawn at various time points (0, 15, 30, 60,  
5 and 120 min), quenched with acetonitrile, filtered, and evaluated via analytical HPLC. The  
6 percent parent compound remaining was determined by integrating the area under the curve and  
7 comparing this number with the initial sample of parent compound at an incubation time of 0  
8 min. Approximately 72% of SAHA-TAP remained after 1 h incubation at 37 °C while only  
9 ~60% of SAHA remained under identical conditions. Only ~50% of either parent compound  
10 remained after a 2 h incubation at 37 °C (Figure 6a). After 2 h incubation at 37 °C the HPLC  
11 trace of SAHA-TAP showed that the major degradation peak (~23%) corresponds to SAHA with  
12 ~52% SAHA-TAP remaining and ~25% other products. This suggests that hydrolysis of SAHA-  
13 TAP to SAHA is a major component of the degradation process in human plasma (Figure S9).  
14 For comparison, after a 2 h incubation in human plasma under identical conditions, the HPLC  
15 chromatogram for SAHA shows the emergence of a series of new unidentifiable peaks (~45%)  
16 with ~55% SAHA remaining (Figure S9). Even though SAHA-TAP gradually degrades over  
17 this 2 h period, it is relatively slow and results in the release of the active drug SAHA. Efforts to  
18 identify other product peaks via LCMS were inconclusive. Overall, this study indicates that  
19 SAHA-TAP has a moderately improved stability profile than SAHA in human plasma.  
20  
21  
22  
23  
24  
25  
26  
27  
28  
29  
30  
31  
32  
33  
34  
35  
36  
37  
38  
39  
40  
41  
42  
43  
44  
45

### 46 Cell Proliferation Studies

47  
48 With the kinetics of activation and plasma stability of SAHA-TAP elucidated, we then studied  
49 the effect of SAHA-TAP on the proliferation of a variety of cell lines. Because SAHA is FDA  
50 approved for CTCL, we selected HH (CTCL) and Jurkat (T-cell leukemia) cell lines for analysis.  
51  
52 The viability of NIH/3T3 (mouse embryo fibroblast) was also tested to determine the toxicity of  
53  
54  
55  
56  
57  
58  
59  
60

1  
2  
3 each compound for a non-cancer cell line. The  $EC_{50}$  values of SAHA, SAHA-TAP, and SAHA-  
4  
5  
6  
7  
8  
9  
10  
11  
12  
13  
14  
15  
16  
17  
18  
19  
20  
21  
22  
23  
24  
25  
26  
27  
28  
29  
30  
31  
32  
33  
34  
35  
36  
37  
38  
39  
40  
41  
42  
43  
44  
45  
46  
47  
48  
49  
50  
51  
52  
53  
54  
55  
56  
57  
58  
59  
60

each compound for a non-cancer cell line. The  $EC_{50}$  values of SAHA, SAHA-TAP, and SAHA-OBn are shown in Figure 6b for each cell line. The observed  $EC_{50}$  values of SAHA for HH and for Jurkat cell lines were  $1.03 \pm 0.21 \mu\text{M}$  and  $1.66 \pm 0.14 \mu\text{M}$ , respectively, consistent with previously reported data.<sup>32, 33</sup> SAHA-TAP is ~3-4-fold less potent than SAHA, but is still an active compound, with calculated  $EC_{50}$  values of  $3.38 \pm 0.30 \mu\text{M}$  and  $6.05 \pm 0.14 \mu\text{M}$  for HH and Jurkat cells, respectively. This difference in potency may be attributed to the alkylated Cys affecting the binding of SAHA to HDAC8; further structural studies are needed to confirm this hypothesis. Interestingly, SAHA also is toxic for NIH/3T3 cell lines, with a calculated  $EC_{50}$  of  $4.80 \pm 0.99 \mu\text{M}$ . Other studies also report cytotoxicity of healthy kidney cells (Vero) after treatment with SAHA ( $EC_{50} = 5.20 \pm 0.96 \mu\text{M}$ ).<sup>28</sup> Unfortunately, cell proliferation studies indicate that SAHA-TAP is also slightly toxic for NIH/3T3 cells with an apparent  $EC_{50}$  value of  $9.37 \pm 1.21 \mu\text{M}$ . As expected, cell proliferation is unaffected by the addition of SAHA-OBn for all cells studied.

### Intracellular Target Validation

With the cell proliferation data in hand for both Jurkat and HH cells, we sought to validate the intracellular target of SAHA-TAP using western blotting techniques. Broad-spectrum HDACi are known to increase the steady-state accumulation of tubulin, an endogenous HDAC substrate and a common marker for intracellular HDAC6 activity.<sup>34, 35</sup> For these experiments, SAHA was used as a positive control, since it has been shown to dramatically increase tubulin acetylation in a variety of cells.<sup>33, 36</sup> Indeed, we observed that SAHA-TAP increased tubulin acetylation in both Jurkat and HH cells without disturbing actin levels (Figure 6c), suggesting that the

antiproliferative mechanism of action for SAHA-TAP, like SAHA, involves nonspecific HDAC inhibition.

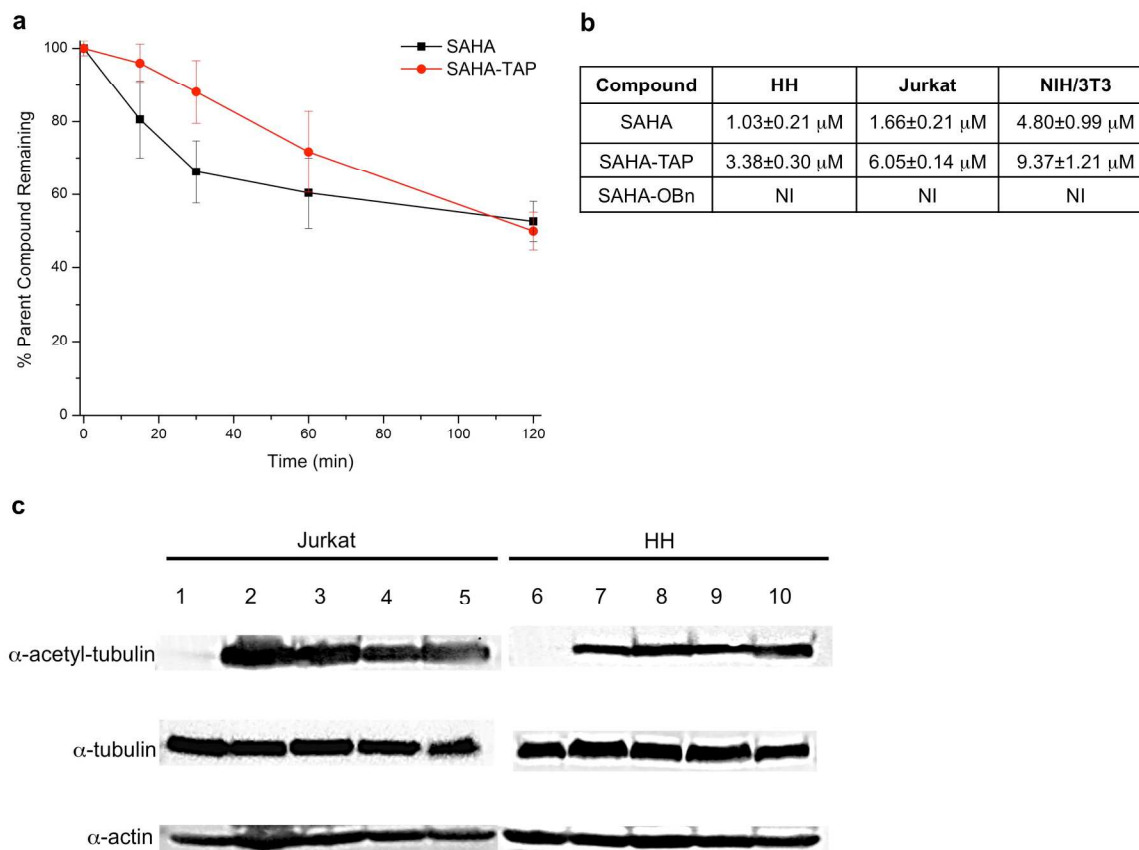


**Figure 6.** (a) Plasma stability for SAHA (red circles) and SAHA-TAP (black squares) over time (mean  $\pm$  sd). (b) Cellular  $EC_{50}$  values ( $\mu$ M) obtained from the MTS cell proliferation assay. NI = no inhibition at 50  $\mu$ M. (c) Western blot analysis of tubulin acetylation for Jurkat (lanes 1-5) and HH (lanes 6-10) cells. Lane 1, control (no treatment); lane 2, SAHA (1.5  $\mu$ M); lane 3, SAHA (20  $\mu$ M); lane 4, SAHA-TAP (6  $\mu$ M); lane 5, SAHA-TAP (20  $\mu$ M); lane 6, control (no treatment); lane 7, SAHA (1.5  $\mu$ M); lane 8, SAHA (20  $\mu$ M); lane 9, SAHA-TAP (6  $\mu$ M); lane 10, SAHA-TAP (20  $\mu$ M).

## Conclusions

A thiol-sensitive prodrug of the FDA-approved HDACi SAHA has been developed that displays a time-dependent inhibition of HDAC8. SAHA-TAP functions as a dual-mode HDAC inhibitor with both a covalent modification and a non-covalent, conventional mode of action. SAHA-TAP is susceptible to nucleophilic attack by Cys residues on the target HDAC, particularly the conserved Cys153 residue in the catalytic domain. These Cys residues are covalently modified with the promoiety, inactivating the enzyme, followed by the release of the competitive inhibitor SAHA. Proteomic MS confirms that this modification occurs at Cys153, and the kinetics of inhibition show unambiguous time-dependent inhibition of HDAC8 by SAHA-TAP, indicative of a covalent modification with release of SAHA. The HDAC8 C153A mutant retains the non-covalent mode of inhibition by SAHA-TAP (Scheme 1), while the time-dependent mode of inhibition disappears. This result demonstrates the importance of the active site Cys in the inactivation of HDAC8 by SAHA-TAP. The stability of SAHA-TAP in human plasma is slightly improved with slow conversion to SAHA observed. In contrast, SAHA is rapidly degraded to several products under identical conditions, consistent with previous literature studies. Finally, cellular proliferation studies show a clear dose-response relationship with SAHA-TAP for two distinct cancer cell lines, with only moderately inferior  $EC_{50}$  values compared to SAHA; immunoblotting confirms that the antiproliferative mechanism of action of SAHA-TAP involves HDAC inhibition. To the best of our knowledge, SAHA-TAP is the first dual-mode HDAC proinhibitor that exploits the modification of an endogenous, conserved Cys residues, namely the catalytic site Cys153 residue in HDAC8, to generate a covalent adduct in addition to releasing a competitive inhibitor.

## Experimental Section

**Enzyme Inhibition Assays.** HDAC-1, -2, -3, -6 and -8 activity was determined in vitro with an optimized homogenous assay performed in a 384-well plate. Recombinant, full-length HDAC protein (BPS Biosciences) was incubated with fluorophore conjugated substrate, MAZ1600 and MAZ1675, at [Substrate] =  $K_m$  (MAZ1600; 11  $\mu\text{M}$  for HDAC1, 18  $\mu\text{M}$  for HDAC2, 9  $\mu\text{M}$  for HDAC3, 4  $\mu\text{M}$  for HDAC6; MAZ1675; 263  $\mu\text{M}$  for HDAC8). Reactions were performed in assay buffer (50 mM HEPES, 100 mM KCl, 0.001% Tween-20, 0.05% BSA and pH 7.4. Additional 200  $\mu\text{M}$  TCEP was added for HDAC6) and followed by fluorogenic release of 7-amino-4-methylcoumarin from substrate upon deacetylase and trypsin enzymatic activity. Fluorescence measurements were obtained every five minutes using a multilabel plate reader and plate-stacker (Envision; Perkin-Elmer). Each plate was analyzed by plate repeat, and the first derivative within the linear range was imported into analytical software (Spotfire DecisionSite). Replicate experimental data from incubations with inhibitor were normalized to DMSO controls ([DMSO] < 0.5%).  $IC_{50}$  values are determined by logistic regression with unconstrained maximum and minimum values.

**Mass Spectrometry Experiments. Preparation.** An aliquot of HDAC8 (1.7  $\mu\text{M}$ ) was incubated with SAHA-TAP (12 eq, 20  $\mu\text{M}$ ) at 37  $^{\circ}\text{C}$  for 1 h. The protein was purified by SDS-PAGE followed by Commassie staining prior to analysis.

**In Gel Digest.** The gel slices of interest were cut to 1 mm cubes and destained 3 times by first washing with 100 mM ammonium bicarbonate (100  $\mu\text{L}$ ) for 15 minutes, followed by the addition of ACN (100  $\mu\text{L}$ ) for 15 minutes. The supernatant was collected and samples were dried in a

1  
2  
3 speedvac. The samples were then reduced by the addition of 100  $\mu$ M ammonium bicarbonate-10  
4 mM DTT (200  $\mu$ L) and incubated at 56  $^{\circ}$ C for 30 min. The liquid was removed and 100 mM  
5 ammonium bicarbonate-55 mM iodoacetamide (200  $\mu$ L) was added to gel pieces and incubated  
6 at RT in the dark for 20 min. After the removal of the supernatant and one wash with 100 mM  
7 ammonium bicarbonate for 15 min, the same volume of ACN was added to dehydrate the gel  
8 pieces. The solution was then removed and the samples were dried in a speedvac. For digestion,  
9 enough solution of ice-cold trypsin (0.01 mg/mL) in 50 mM ammonium bicarbonate was added  
10 to cover the gel pieces, and then incubated on ice for 30 min. After complete rehydration, the  
11 excess trypsin solution was removed, replaced with fresh 50 mM ammonium bicarbonate, and  
12 incubated overnight at 37  $^{\circ}$ C. The peptides were extracted twice by the addition of 0.2% formic  
13 acid and 5% ACN (50  $\mu$ L) and vortex mixing at RT for 30 min. The supernatant was removed  
14 and saved. A total of 50  $\mu$ L of 50% ACN-0.2% formic acid was added to the sample, which was  
15 vortexed again at RT for 30 min. The supernatant was removed and combined with the  
16 supernatant from the first extraction. The combined extractions were analyzed directly by LCMS.

17  
18  
19  
20  
21  
22  
23  
24  
25  
26  
27  
28  
29  
30  
31  
32  
33  
34  
35  
36  
37 **LC-MS/MS.** Trypsin-digested peptides were analyzed by HPLC coupled with tandem mass  
38 spectrometry (LC-MS/MS) using nano-spray ionization. The nanospray ionization experiments  
39 were performed using a TripleTOF 5600 hybrid mass spectrometer (SCIEX) interfaced with  
40 nano-scale reversed-phase HPLC (Tempo) using a 10 cm-100 micron ID glass capillary packed  
41 with 5-mm C18 Zorbax<sup>TM</sup> beads (Agilent Technologies). Peptides were eluted from the C18  
42 column into the mass spectrometer using a linear gradient (5–60%) of ACN at a flow rate of 250  
43 mL/min for 1 h. The buffers used to create the ACN gradient are: Buffer A (98% H<sub>2</sub>O, 2%  
44 ACN, 0.2% formic acid, and 0.005% TFA) and Buffer B (0.2% formic acid and 0.005% TFA in  
45 ACN). MS/MS data were acquired in a data-dependent manner in which the MS1 data was  
46  
47  
48  
49  
50  
51  
52  
53  
54  
55  
56  
57  
58  
59  
60



1  
2  
3 acquired for 250 ms at  $m/z$  of 400 to 1250 Da and the MS/MS data was acquired from  $m/z$  of 50  
4  
5 to 2,000 Da. For Independent data acquisition (IDA) parameters MS1-TOF 250 milliseconds,  
6  
7 followed by 50 MS2 events of 25 milliseconds each. The IDA criteria, over 200 counts  
8  
9 threshold, charge state +2-4 with 4 seconds exclusion. Finally, the collected data were analyzed  
10  
11 using MASCOT<sup>®</sup> (Matrix Sciences).  
12  
13  
14  
15  
16

17 **Protein Expression and Purification.** Recombinant human HDAC8 in a pET-20b-derived  
18  
19 plasmid with an added c-terminal TEV protease cleavage site and His<sub>6</sub> tag (termed pHD)<sup>28</sup> was  
20  
21 expressed and purified in *E.coli* BL21(DE3) according to Gantt and coworkers,<sup>28</sup> with the  
22  
23 following modification: elution from the nickel columns was performed using a linear gradient  
24  
25 (10-250 mM imidazole). In the preparation of apo-enzyme, HDAC8 was dialyzed twice at 4 °C  
26  
27 against 4 L of 25 mM MOPS, 1 mM EDTA, 5 mM KCl, 1 mM TCEP, pH 7.5 followed by four  
28  
29 times against 2 L of 25 mM MOPS, 5 mM KCl, 1 mM TCEP, pH 7.5. All components were free  
30  
31 of transition metals and dialysis occurred in plasticware that had been washed with EDTA and  
32  
33 rinsed with Milli-Q ddH<sub>2</sub>O. Apo-enzyme was stored at -80 °C in the same metal-free buffer.  
34  
35 The Cys153Ala HDAC8 mutant was constructed in a pHD4 TEV-His plasmid, using the  
36  
37 QuikChange site-directed mutagenesis protocol and kit, and the mutation was confirmed by the  
38  
39 UM DNA sequencing facility. This construct was expressed and purified in the same manner as  
40  
41 wild-type enzyme.  
42  
43  
44  
45  
46  
47  
48  
49  
50

51 **HDAC8 Time-course Inhibition Experiments.** Recombinant WT or C153A mutant human  
52  
53 HDAC8 was reconstituted for 1 h on ice at a 1:1 stoichiometry (at 10 μM) with Zn<sup>2+</sup> in 1×  
54  
55 HDAC assay buffer (25 mM HEPES, 3 mM KCl, 137 mM NaCl, pH 8.0). The 5 and 50 mM  
56  
57  
58  
59  
60

1  
2  
3 SAHA-TAP, SAHA-OBn, and SAHA stocks were serially diluted into decreasing concentrations  
4  
5 of DMSO to maintain solubility of the compounds. Reaction mixtures of 1× HDAC assay  
6  
7 buffer, 150 μM Fluor-de-Lys peptide substrate (R – H – K(Ac) - K(Ac) - fluorophore) (Enzo  
8  
9 Life Sciences), and various concentrations of inhibitors (SAHA-TAP, SAHA-OBn, or SAHA)  
10  
11 were prepared and allowed to equilibrate at 30 °C. The final DMSO content was <1%. Assays  
12  
13 were initiated by addition of wild-type (0.5 μM) or Cys153Ala mutant (2 μM) HDAC8. At  
14  
15 various time points a reaction aliquot (5 μL) was diluted into a Fluor-de-Lys quench solution (45  
16  
17 μL) containing trypsin and trichostatin A (TSA). Assays were read in 96-well plates (Corning  
18  
19 3686) using a PolarStar Fluorescent plate reader. The fluorescence corresponding to product  
20  
21 formation ( $\lambda_{\text{ex}} = 340 \text{ nm}$ ,  $\lambda_{\text{em}} = 450 \text{ nm}$ ) and remaining substrate ( $\lambda_{\text{ex}} = 340 \text{ nm}$ ,  $\lambda_{\text{em}} = 380 \text{ nm}$ )  
22  
23 was measured and the ratio of product formed/remaining substrate is reported. Standard curves  
24  
25 demonstrate that this fluorescent ratio linearly reflects product under these conditions.  
26  
27  
28  
29  
30  
31  
32  
33  
34

35 **Cell Proliferation Studies.** HH and Jurkat cell lines were obtained from ATCC (Manassas,  
36  
37 VA, USA), and grown on RPMI 1640 medium supplemented with 10% fetal bovine serum  
38  
39 (Gibco, Grand Island, NY, USA). The NIH/3T3 cell line was kindly donated by Dr. Richard  
40  
41 Klemke and grown on DMEM medium supplemented with 10% fetal bovine serum (Gibco,  
42  
43 Grand Island, NY, USA) at 37 °C in an incubator with 5% CO<sub>2</sub>. The CellTiter 96 AQueous One  
44  
45 Solution Cell Proliferation assay (MTS) kit was purchased from Promega (Madison, WI, USA).  
46  
47 Cell viability was measured using the MTS assay according to the manufacturer protocol. To  
48  
49 start the assay, cells were counted with a hemocytometer, diluted with fresh medium to the  
50  
51 proper concentration and seeded in 96 well plates (5000 cells/well for NIH/3T3 and 20000  
52  
53 cells/well for HH and Jurkat). Jurkat and HH cells were then directly incubated in media  
54  
55  
56  
57  
58  
59  
60

1  
2  
3 containing the various concentrations of drugs for 70 h (ranging from 0.5  $\mu\text{M}$  to 128  $\mu\text{M}$ ).  
4  
5 NIH/3T3 cells were first incubated at 37 °C with 5%  $\text{CO}_2$  for 16 h prior to the drug treatment for  
6  
7 cell attachment. The cells were then treated with various concentrations of drugs for 70 h. The  
8  
9 CellTiter 96 AQueous One Solution was added (20  $\mu\text{L}$  per well) and the plate was incubated at  
10  
11 37 °C for 2 h (NIH 3T3) or 4 h (HH and Jurkat). The absorbance was recorded at 490 nm using  
12  
13 the BioTek Synergy HT microplate reader. Each concentration of drug treatment was conducted  
14  
15 in triplicate for each trail with 2-3 trials conducted.  
16  
17  
18  
19  
20  
21

22 **Plasma Stability.** The plasma stability of SAHA and SAHA-TAP was investigated with  
23  
24 pooled normal human plasma (Innovative Research, Novi, MI). In duplicate, plasma (1.0 mL)  
25  
26 was pre-incubated for 2 min at 37 °C followed by the addition of 20  $\mu\text{L}$  of a 5.0 mM stock  
27  
28 solution (DMSO). Aliquots (100  $\mu\text{L}$ ) were withdrawn at 0, 15, 30, 60, and 120 min and  
29  
30 immediately quenched with 100  $\mu\text{L}$  ACN to precipitate the proteins. The samples were vortexed  
31  
32 thoroughly and centrifuged for 2 min at 13,000 RPM. The supernatant was collected and  
33  
34 centrifuged through 0.2  $\mu\text{m}$  spin filters (Corning) for 5 min at 8,000 RPM. Samples were then  
35  
36 frozen until analyzed by HPLC with the following method: Analytical HPLC was performed on  
37  
38 a HP Series 1050 System equipped with a Poroshell 120 reverse-phase column (EC-C18,  
39  
40 4.6 $\times$ 100 mm, 2.7  $\mu\text{m}$ ). Separation was achieved with a flow rate of 1  $\text{mL min}^{-1}$  and the  
41  
42 following mobile phase: 2.5% ACN + 0.1% formic acid in  $\text{H}_2\text{O}$  (A) and 0.1% formic acid in  
43  
44 ACN (B). Starting with 95% A and 5% B, a linear gradient was run for 15 min to a final solvent  
45  
46 mixture of 5% A and 95% B, which was held for 5 min before ramping back down to 95% A and  
47  
48 5% B over the course of 2 min, with constant holding at this level for 4 additional min.  
49  
50  
51  
52  
53  
54  
55  
56  
57  
58  
59  
60

1  
2  
3 **Western Blot Analysis.** Log phase growing HH and Jurkat cell lines were cultured until 70%  
4 percent confluent and treated with specified concentrations of compounds for 4 hours prior to  
5 harvesting. Cells were spun at 250 x g and washed with DPBS buffer (Life Technologies) before  
6 lysis using RIPA Buffer (50 mM Tris-HCl (pH 7.5), 150 mM Na<sub>2</sub>EDTA, 1% Nonidet P-40, 1%  
7 sodium deoxycholate, 0.1% sodium dodecyl sulphate) supplanted with cOmplete protease  
8 inhibitors cocktail (Roche) for 30 min on ice. Samples were then spun at 12,000 x g before  
9 quantification of total protein concentration using a BCA assay (Thermo). Dilutions were made  
10 to normalize total protein concentration for each gel sample. Diluted samples were then run on a  
11 10% SDS-PAGE gel at 100 V for 2 h before transfer onto Immobilon-P PVDF Membrane (EMD  
12 Millipore) at 100 V for 45 min before blocking in 5% (v/v) Casein-TBST (Tris-buffered saline  
13 Tween-20; 0.05% Tween-20 v/v) at 4 °C. Blots were then incubated with monoclonal mouse  
14 anti-acetylated tubulin (Life Technologies), polyclonal rabbit anti-tubulin (Sigma), or anti-actin-  
15 HRP (Santa Cruz) in 5% (v/v) BSA-TBST at dilutions according to manufacturer instructions  
16 overnight at 4 °C. Blots were then washed by three 5 min washes in TBST (0.05% v/v) anti-  
17 acetylated tubulin and anti-tubulin antibodies were then incubated with HRP-conjugated anti-  
18 mouse (Santa Cruz) or anti-rabbit (Pierce). Detection was performed using SuperSignal West  
19 Pico Substrate (Pierce) with 10% (v/v) SuperSignal West Femto Substrate (Pierce) and imaged  
20 on ChemiDoc XRS+ System with Image Lab Software (Bio-rad).  
21  
22  
23  
24  
25  
26  
27  
28  
29  
30  
31  
32  
33  
34  
35  
36  
37  
38  
39  
40  
41  
42  
43  
44  
45  
46  
47

#### 48 ASSOCIATED CONTENT

49  
50  
51 **Supporting Information.** Synthetic procedures, NMR and MS characterization, analytical  
52 HPLC chromatograms, enzyme inhibition assay results, progress curves, and proteomic MS data.  
53  
54 This material is available free of charge via the Internet at <http://pubs.acs.org>.  
55  
56  
57  
58  
59  
60

## AUTHOR INFORMATION

\* To whom correspondence should be addressed.

E-mail: scohen@ucsd.edu. Telephone: (858) 822-5596

E-mail: fierke@umich.edu. Telephone: (734) 936-2678

**Author Contributions**

K.B.D. conceived the project, synthesized all compounds, and designed and performed experiments. E.D.S. designed experiments, expressed/purified WT HDAC8 and C153A mutant HDAC8, and performed all time-dependent progress curve experiments. Y.C. performed all cell proliferation experiments. J.C.C. performed all western blot experiments. K.B.D., E.D.S., Y.C., J.C.C., P.A.J., C.A.F., and S.M.C. analyzed the data and wrote the manuscript.

## ACKNOWLEDGMENT

The authors would like to acknowledge the James E. Bradner laboratory for performing preliminary HDAC inhibition studies, and Dr. Majid Ghassemian (UCSD Biomolecular and Proteomics MS Facility) for completing proteomic MS experiments. The authors would also like to thank Dr. David P. Martin and Dr. David T. Puerta for helpful discussions. This work was supported by grants from the US National Institutes of Health (NIH) through the National Institute of General Medical Sciences (NIGMS) (R01 GM101467; P.A.J.), (R01 GM40602; C.A.F.), and (R01 GM098435; S.M.C.).

## ABBREVIATIONS

HDAC, Histone Deacetylase; HDACi, Histone Deacetylase Inhibitor; PK, pharmacokinetics; CTCL, Cutaneous T-Cell Lymphoma; GSH, Glutathione in its reduced form; Cys, Cysteine.

## REFERENCES

1. Haberland, M.; Montgomery, R. L.; Olson, E. N. The many roles of histone deacetylases in development and physiology: implications for disease and therapy. *Nat. Rev. Genet.* **2009**, *10*, 32-42.
2. De Ruijter, A. J. M.; Van Gennip, A. H.; Caron, H. N.; Kemp, S.; Van Kuilenburg, A. B. P. Histone deacetylases (HDACs): characterization of the classical HDAC family. *Biochem. J.* **2003**, *370*, 737-749.
3. Marks, P. A.; Rifkind, R. A.; Richon, V. M.; Breslow, R.; Miller, T.; Kelly, W. K. Histone deacetylases and cancer: Causes and therapies. *Nat. Rev. Cancer* **2001**, *1*, 194-202.
4. Johnstone, R. W. Histone-deacetylase inhibitors: Novel drugs for the treatment of cancer. *Nat. Rev. Drug Discov.* **2002**, *1*, 287-299.
5. Agaloti, T.; Chen, G.; Thanos, D. Deciphering the Transcriptional Histone Acetylation Code for a Human Gene. *Cell* **2002**, *111*, 381-392.

- 1  
2  
3  
4  
5  
6  
7  
8  
9  
10  
11  
12  
13  
14  
15  
16  
17  
18  
19  
20  
21  
22  
23  
24  
25  
26  
27  
28  
29  
30  
31  
32  
33  
34  
35  
36  
37  
38  
39  
40  
41  
42  
43  
44  
45  
46  
47  
48  
49  
50  
51  
52  
53  
54  
55  
56  
57  
58  
59  
60
6. Matangkasombut, O.; Buratowski, S. Different sensitivities of bromodomain factors 1 and 2 to histone H4 acetylation. *Mol. Cell.* **2003**, 11, 353-363.
  7. Choudhary, C.; Kumar, C.; Gnad, F.; Nielsen, M. L.; Rehman, M.; Walther, T. C.; Olsen, J. V.; Mann, M. Lysine Acetylation Targets Protein Complexes and Co-Regulates Major Cellular Functions. *Science* **2009**, 325, 834-840.
  8. Gryder, B. E.; Sodji, Q. H.; Oyelere, A. K. Targeted cancer therapy: giving histone deacetylase inhibitors all they need to succeed. *Future Med. Chem.* **2012**, 4, 505-524.
  9. Dokmanovic, M.; Clarke, C.; Marks, P. A. Histone deacetylase inhibitors: Overview and perspectives. *Mol. Cancer Res.* **2007**, 5, 981-989.
  10. Kantharaj, E.; Jayaraman, R. *Hisono Deacetylase Inhibitors as Therapeutic Agents for Cancer Therapy*. Intech: Rijeka, Croatia, 2011.
  11. Marks, P. A.; Breslow, R. Dimethyl sulfoxide to vorinostat: Development of this histone deacetylase inhibitor as an anticancer drug. *Nat. Biotechnol.* **2007**, 25, 84-90.
  12. <http://www.fda.gov/NewsEvents/Newsroom/PressAnnouncements/ucm435296.htm>. FDA approves Farydak for treatment of multiple myeloma. **2015**.
  13. <http://www.fda.gov/Drugs/InformationOnDrugs/ApprovedDrugs/ucm403960.htm>. Belinostat. **2014**.

- 1  
2  
3 14. Rubin, E. H.; Agrawal, N. G. B.; Friedman, E. J.; Scott, P.; Mazina, K. E.; Sun, L.; Du, L.  
4  
5 H.; Ricker, J. L.; Frankel, S. R.; Gottesdiener, K. M.; Wagner, J. A.; Iwamoto, M. A study to  
6  
7 determine the effects of food and multiple dosing on the pharmacokinetics of vorinostat given  
8  
9 orally to patients with advanced cancer. *Clin. Cancer Res.* **2006**, 12, 7039-7045.  
10  
11  
12  
13  
14 15. Flipo, M.; Charton, J.; Hocine, A.; Dassonneville, S.; Deprez, B.; Deprez-Poulain, R.  
15  
16 Hydroxamates: Relationships between Structure and Plasma Stability. *J. Med. Chem.* **2009**, 52,  
17  
18 6790-6802.  
19  
20  
21  
22  
23 16. Andreu-Vieyra, C. V.; Berenson, J. R. The potential of panobinostat as a treatment  
24  
25 option in patients with relapsed and refractory multiple myeloma. *Ther. Adv. Hematol.* **2014**, 5,  
26  
27 197-210.  
28  
29  
30  
31 17. Rautio, J.; Kumpulainen, H.; Heimbach, T.; Oliyai, R.; Oh, D.; Jarvinen, T.; Savolainen,  
32  
33 J. Prodrugs: design and clinical applications. *Nat. Rev. Drug Discov.* **2008**, 7, 255-270.  
34  
35  
36  
37  
38 18. Huttunen, K. M.; Raunio, H.; Rautio, J. Prodrugs-from Serendipity to Rational Design.  
39  
40 *Pharm. Rev.* **2011**, 63, 750-771.  
41  
42  
43  
44 19. Miller, T. A.; Witter, D. J.; Belvedere, S. Histone Deacetylase Inhibitor Prodrugs. April 5,  
45  
46 2005, 2005.  
47  
48  
49  
50 20. Schlimme, S.; Hauser, A. T.; Carafa, V.; Heinke, R.; Kannan, S.; Stolfa, D. A.;  
51  
52 Cellamare, S.; Carotti, A.; Altucci, L.; Jung, M.; Sippl, W. Carbamate Prodrug Concept for  
53  
54 Hydroxamate HDAC Inhibitors. *ChemMedChem* **2011**, 6, 1193-1198.  
55  
56  
57  
58  
59  
60



- 1  
2  
3  
4  
5  
6  
7  
8  
9  
10  
11  
12  
13  
14  
15  
16  
17  
18  
19  
20  
21  
22  
23  
24  
25  
26  
27  
28  
29  
30  
31  
32  
33  
34  
35  
36  
37  
38  
39  
40  
41  
42  
43  
44  
45  
46  
47  
48  
49  
50  
51  
52  
53  
54  
55  
56  
57  
58  
59  
60
21. Estrela, J. M.; Ortega, A.; Obrador, E. Glutathione in cancer biology and therapy. *Crit. Rev. Clin. Lab Sci.* **2006**, 43, 143-181.
22. Huang, S. T.; Ting, K. N.; Wang, K. L. Development of a long-wavelength fluorescent probe based on quinone-methide-type reaction to detect physiologically significant thiols. *Anal. Chim. Acta* **2008**, 620, 120-126.
23. Thomas, M.; Rivault, F.; Tranoy-Opalinski, I.; Roche, J.; Gesson, J.-P.; Papot, S. Synthesis and biological evaluation of the suberoylanilide hydroxamic acid (SAHA)  $\beta$ -glucuronide and  $\beta$ -galactoside for application in selective prodrug chemotherapy. *Bioorg. Med. Chem. Lett.* **2007**, 17, 983-986.
24. Kelly, W. K.; Richon, V. M.; O'Connor, O.; Curley, T.; MacGregor-Curtelli, B.; Tong, W.; Klang, M.; Schwartz, L.; Richardson, S.; Rosa, E.; Drobnjak, M.; Cordon-Cordo, C.; Chiao, J. H.; Rifkind, R.; Marks, P. A.; Scher, H. Phase I clinical trial of histone deacetylase inhibitor: Suberoylanilide hydroxamic acid administered intravenously. *Clin. Cancer Res.* **2003**, 9, 3578-3588.
25. Furumai, R.; Matsuyama, A.; Kobashi, N.; Lee, K. H.; Nishiyama, N.; Nakajima, I.; Tanaka, A.; Komatsu, Y.; Nishino, N.; Yoshida, M.; Horinouchi, S. FK228 (depsipeptide) as a natural prodrug that inhibits class I histone deacetylases. *Cancer Res.* **2002**, 62, 4916-4921.
26. Kim, B.; Pithadia, A. S.; Fierke, C. A. Kinetics and thermodynamics of metal-binding to histone deacetylase 8. *Protein Sci.* **2015**, 24, 354-65.
27. McLafferty, F. W. Tandem Mass-Spectrometry. *Science* **1981**, 214, 280-287.

- 1  
2  
3 28. Gantt, S. L.; Gattis, S. G.; Fierke, C. A. Catalytic activity and inhibition of human histone  
4 deacetylase 8 is dependent on the identity of the active site metal ion. *Biochemistry-Us* **2006**,  
5 45, 6170-6178.  
6  
7  
8  
9  
10  
11 29. McClerren, A. L.; Endsley, S.; Bowman, J. L.; Andersen, N. H.; Guan, Z.; Rudolph, J.;  
12 Raetz, C. R. A slow, tight-binding inhibitor of the zinc-dependent deacetylase LpxC of lipid A  
13 biosynthesis with antibiotic activity comparable to ciprofloxacin. *Biochemistry-Us* **2005**, 44,  
14 16574-83.  
15  
16  
17  
18  
19  
20  
21  
22 30. Sculley, M. J.; Morrison, J. F.; Cleland, W. W. Slow-binding inhibition: the general case.  
23 *Biochim. Biophys. Acta* **1996**, 1298, 78-86.  
24  
25  
26  
27  
28  
29 31. Teitelbaum, A. M.; Meissner, A.; Harding, R. A.; Wong, C. A.; Aldrich, C. C.; Rimmel, R.  
30 P. Synthesis, pH-dependent, and plasma stability of meropenem prodrugs for potential use  
31 against drug-resistant tuberculosis. *Bioorg. Med. Chem.* **2013**, 21, 5605-5617.  
32  
33  
34  
35  
36  
37 32. Zhang, C. L.; Richon, V.; Ni, X.; Talpur, R.; Duvic, M. Selective induction of apoptosis by  
38 histone deacetylase inhibitor SAHA in cutaneous T-cell lymphoma cells: Relevance to  
39 mechanism of therapeutic action. *J. Invest. Dermatol.* **2005**, 125, 1045-1052.  
40  
41  
42  
43  
44  
45 33. Sodji, Q. H.; Patil, V.; Kornacki, J. R.; Mrksich, M.; Oyelere, A. K. Synthesis and  
46 Structure-Activity Relationship of 3-Hydroxypyridine-2-thione-Based Histone Deacetylase  
47 Inhibitors. *J. Med. Chem.* **2013**, 56, 9969-9981.  
48  
49  
50  
51  
52  
53  
54 34. Zhang, Y.; Li, N.; Caron, C.; Matthias, G.; Hess, D.; Khochbin, S.; Matthias, P. HDAC-6  
55 interacts with and deacetylates tubulin and microtubules in vivo. *EMBO J.* **2003**, 22, 1168-79.  
56  
57  
58  
59  
60

1  
2  
3 35. Bantscheff, M.; Hopf, C.; Savitski, M. M.; Dittmann, A.; Grandi, P.; Michon, A. M.;  
4  
5 Schlegl, J.; Abraham, Y.; Becher, I.; Bergamini, G.; Boesche, M.; Delling, M.; Dumpelfeld, B.;  
6  
7 Eberhard, D.; Huthmacher, C.; Mathieson, T.; Poeckel, D.; Reader, V.; Strunk, K.; Sweetman,  
8  
9 G.; Kruse, U.; Neubauer, G.; Ramsden, N. G.; Drewes, G. Chemoproteomics profiling of HDAC  
10  
11 inhibitors reveals selective targeting of HDAC complexes. *Nat Biotechnol* **2011**, 29, 255-65.  
12  
13

14  
15  
16 36. Gryder, B. E.; Akbashev, M. J.; Rood, M. K.; Raftery, E. D.; Meyers, W. M.; Dillard, P.;  
17  
18 Khan, S.; Oyelere, A. K. Selectively targeting prostate cancer with antiandrogen equipped  
19  
20 histone deacetylase inhibitors. *ACS Chem. Biol.* **2013**, 8, 2550-60.  
21  
22  
23  
24  
25  
26  
27  
28  
29  
30  
31  
32  
33  
34  
35  
36  
37  
38  
39  
40  
41  
42  
43  
44  
45  
46  
47  
48  
49  
50  
51  
52  
53  
54  
55  
56  
57  
58  
59  
60

## Table of Contents graphic.

